HEFAT2012
9th International Conference on Heat Transfer, Fluid Mechanics and Thermodynamics
16 – 18 July 2012
Malta

ENHANCED HEAT TRANSFER IN LAMINAR PULSATING FLOW PAST A FLAT PLATE

Cárdenas Miranda, A.* and Polifke, W.
*Author for correspondence

Lehrstuhl für Thermodynamik,
Technische Universität München,
Munich, Germany,
E-mail: cardenas@td.mw.tum.de

ABSTRACT

Heat transfer in laminar pulsating flow past a heated flat plate is investigated. In contrast to previous investigations, the response of the wall heat flux to both harmonic velocity and temperature fluctuations is considered over a wide range of pulsation amplitudes and Strouhal numbers. The reason for choosing the flat plate configuration is that for one given oscillation frequency, both low- and high-frequency regimes can be observed in a single simulation. Due to the spatial development of the hydrodynamic and thermal boundary layers along the length of the plate, the Stokes length is first larger (upstream section), then (downstream section) smaller than the local boundary layer thickness. Firstly, the case with constant wall temperature is studied, where fluid temperature fluctuations are locally generated by velocity perturbations in the presence of mean flow gradients. Depending on the local Strouhal number, which controls boundary layer phase lags, the local wall heat flux can be enhanced as well as decreased. This effect is due to a nonlinear interaction between velocity and temperature fluctuations. Secondly, periodic temperature fluctuations of the wall temperature are imposed too, and the deviations from the stationary case are stronger. At high velocity amplitudes, secondary flows induced by viscous forces near stagnation points come into play and can either support or impede the enhancement of heat transfer.

NOMENCLATURE

a	$[m^2/s]$	Thermal diffusivity
c_p	$[W/(kgK)]$	Specific heat capacity
i	[-]	Complex $\sqrt{-1}$
g	[-]	Gain
L	$[m]$	Plate length
Pr	[-]	Prandtl number
$\dot{q}_w$	$[W/m^2]$	Wall heat flux
Re	[-]	Reynolds number
Sr	[-]	Strouhal number
T	$[K]$	Temperature
T_{in}	$[K]$	Bulk temperature
T_w	$[K]$	Wall surface temperature
t	$[s]$	Time
U_0	[m/s]	Bulk velocity
u	[m/s]	Velocity in x direction
v	[m/s]	Velocity in y direction
x	$[m]$	Cartesian axis direction
y	$[m]$	Cartesian axis direction

Special characters

ν	$[m^2/s]$	Dynamic viscosity
μ	$[kg/ms]$	Kinematic viscosity
λ	$[W/mK]$	Thermal conductivity
ω	$[1/s]$	Frequency
ρ	$[kg/m^3]$	Density
δ	$[m]$	Boundary layer thickness
δ_s	$[m]$	Stokes' length
ϵ_u	[-]	Velocity amplitude ratio
ϵ_T	[-]	Temperature amplitude ratio
τ_w	$[N/m^2]$	Skin friction
ξ	[-]	Dimensionless frequency (local Strouhal number)
η	[-]	Wall units

Subscripts

In	Inlet properties
W	Wall properties
Stat	Stationary reference case
n	Harmonic order

Superscripts

*	Dimensionless quantities
$^{\rightarrow}$	Vector

INTRODUCTION

Enhanced heat transfer in transient periodic flows has been reported repeatedly, especially in devices suffering from self-excited combustion oscillations. In the tailpipe of a pulse combustor, Dec et al. [1] measured wall heat fluxes that locally exceeded the expected values by up to 300%. Furthermore, in a triggered solid propellants rocket thrust chamber with large amplitude oscillations, Perry and Culick [2] found that the average heat transfer rate is increased by the oscillations.

Some explanations of this enhanced heat transfer have been suggested in the literature, for example the increase in turbulence intensity or the creation of coherent structures at times of flow reversal [1]. However, the responsible mechanisms have not yet been clarified without doubt. Especially because of the wide range of perturbation amplitudes and mean flow Reynolds numbers used in the different investigations, apparently contradictory arguments can be found in literature, with both enhancement and decrease of heat transfer being reported.

Hemida et al. [4] attempt to clarify this issues with a theoretical analysis of heat transfer in laminar pulsating flow in a tube with constant wall heat flux. They found that the local Nusselt number exhibits a spatial modulation along the tube with both higher and lower values compared to the stationary case. The perturbations are mostly present in the thermally developing region and are damped out further downstream. However, their studies are restricted to pulsating flow without flow reversal.

In an experimental study of laminar pulsating pipe flow, Habib et al. [5] studied the heat transfer characteristics at different pulsation frequencies. They also found cases with higher aswell as lower Nusselt numbers and confirmed that the effects are primarily present in the thermally developing region.

In devices where enhanced heat transfer has been observed, it can be expected that temperature fluctuations occur in addition to the ones of velocity. For example, the bulk temperature of the fluid might oscillate due to combustion instabilities. In an analytical approach, Marksten et al. [3] showed that an interaction of these two fluctuations can indeed lead to considerably enhanced heat transfer in a laminar pulsating pipe flow.

The aim of this study is to further investigate numerically with CFD the heat transfer in laminar pulsating flows. In distinction to earlier studies, fluctuations of both velocity and temperature are considered. Furthermore, high velocity amplitude ratios greater than unity and flow reversal will be covered. The two dimensional case of pulsating flow past a flat plate has been chosen for the numerical investigations. The bulk flow is treated as incompressible with constant properties, constant average velocity and forced harmonic oscillations. Transient thermal boundary conditions at the plate are used to account for their impact to the heat transfer. This configuration has been chosen, because even if the oscillations are forced at one single frequency, the low- and high frequency regimes appear. Since the hydrodynamic and thermal boundary layers grow unobstructedly, their ratio compared to the Stokes' layer of constant thickness will change gradually along the plate.

THEORETICAL BACKGROUND

Pulsating flows have been studied for many years. An extensive review of the literature and state of the art can be found in [6]. Here, only a brief description of the most relevant parameters will be given.

In this report we will limit the investigations to laminar flows at low Mach numbers and small temperature ranges. Thus, the here presented flows can be treated as incompressible with constant material properties. In this case the governing equations can be written as:

$$\frac{\partial \vec{u}}{\partial t} + (\vec{u} \cdot \vec{\nabla})\vec{u} = -\frac{\vec{\nabla} p}{\rho} + \nu \vec{\nabla}^2 \vec{u} \tag{1}$$

$$\frac{\partial T}{\partial t} + (\vec{u} \cdot \vec{\nabla})T = a \vec{\nabla}^2 T \tag{2}$$

with the kinematic viscosity ν and the thermal diffusivity $a = \lambda/(\rho c_p)$. The momentum Equation (1) satisfies the mass conservation $\vec{\nabla} \cdot \vec{u} = 0$. Equation (2) corresponds to a transport equation for the temperature as a passive scalar and is a special simplified form of the energy conservation equation. In this way momentum and energy equations are only weakly coupled since the velocity field is uncoupled from the temperature field, but not the other way around.

The skin friction τ_w is a characteristic quantity for the momentum transfer in laminar boundary flows. The wall heat flux $\dot{q}_w$ characterizes the heat transfer in an analogous manner.

$$\tau_w = \mu \left(\frac{\partial u}{\partial y}\right)_{y=0} \quad , \quad \dot{q}_w = -\lambda \left(\frac{\partial T}{\partial y}\right)_{y=0} \quad . \tag{3}$$

Oscillating Flow

A prime example is the flow over a flat plate that oscillates harmonically in the x direction with velocity amplitude U_0. This simple case, usually referred to as Stokes' second problem, displays already some of the important characteristics of periodic flows. Due to the symmetry of the problem, the momentum equation reduces to:

$$\frac{\partial u}{\partial t} = \nu \frac{\partial^2 u}{\partial y^2} \tag{4}$$

with the boundary conditions of the problem $u \to 0$ as $y \to \infty$ and $u = U_0 e^{i\,\omega t}$ for $y = 0$. Applying an harmonic approach for the y-dependency of the flow velocity u, the general solution of the above problem is given by [7]:

$$u = u_0 \exp\left(-\sqrt{\frac{\omega}{2\,\nu}} y\right) \exp\left(i \sqrt{\frac{\omega}{2\nu}} y\right) \exp(i\omega t) \tag{5}$$

The flow motion induced by the plate oscillations dies exponentially out when moving away from the wall. The amplitude decay rate in the y direction is a typical scale, called "Stokes' length":

$$\delta_s = \sqrt{\frac{2\nu}{\omega}} \quad . \tag{6}$$

Pulsating Flow

Lighthill studied the response of the hydrodynamic and thermal boundary layers to fluctuations of small amplitude in the external flow about a mean value [9]. In the streamwise direction he expresses the external flow (capital letters) with harmonic perturbations as follows:

$$U(x,t) = U_0(x)(1 + \epsilon e^{i\omega t}) \quad , \tag{7}$$

where the perturbations are of order ϵ. He further assumes that the boundary layer velocities (small letters) will perform small harmonic oscillations about a steady mean:

$$u(x,t) = u_0(x) + \hat{u}_1\, e^{i\,\omega\, t} = u_0 + u_1 e^{i\omega t + \phi} \quad , \tag{8}$$

however with a possible phase angle compared to the external flow oscillations. Thus, the amplitude $\hat{u}_1$ can be complex valued. Figure 1 illustrates this behaviour in a polar diagram. The complex vector $\hat{u}_1$ oscillates with the same angular frequency ω as the external flow, but might have a phase lag ϕ. Of course, only the real parts of the expressions represent the physical quantities.

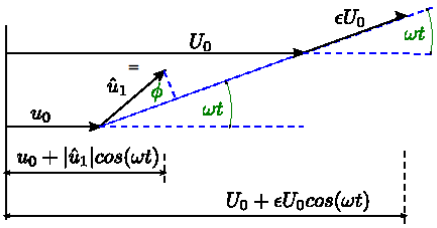

Figure 1 Polar diagram of internal and external velocities, displaying the possible phase lag ϕ **[7]**.

Lighthill solved this problem for two limiting cases. The high frequency approximation is valid for flows with boundary layer thickness much larger than the Stokes' length, $\delta \gg \delta_s$. In this case, the general solution for the velocity in the boundary layer writes:

$$\hat{u}_1 = \epsilon U_0 \left(1 - e^{-y\sqrt{\frac{i\omega}{\nu}}}\right) \quad . \tag{9}$$

Applying the identity $\sqrt{i} = \frac{1}{\sqrt{2}} + \frac{i}{\sqrt{2}}$ the solution given by Equation (16) can be split into real and imaginary parts $\hat{u}_1 = u_r + iu_i$, and the Stokes' Length presented in the previous section appears again:

$$u_r = U_0 \left[1 - e^{-\frac{y}{\delta_s}} \cos\left(\frac{y}{\delta_s}\right)\right], u_i = U_0 e^{-\frac{y}{\delta_s}} \sin\left(\frac{y}{\delta_s}\right). \tag{10}$$

The phase lag can be expressed as:

$$\tan(\phi) = \frac{\sin(y)}{\frac{1}{\delta_s} e^{\delta_s^2} - \cos(y)} \quad . \tag{11}$$

The bounds of the phase lag of the velocity fluctuations are $\pi/4$ for the limiting case $y \to 0$ and 0 for $y \to \infty$. This means that in the high frequency regime, the velocity fluctuations in the boundary layer advance the fluctuations of the external flow. Due to the viscous forces in the boundary layer, the velocity amplitudes are smaller. Thus, the inertia of the fluid in this region is lower and it can respond faster to external perturbations.

The small frequency approximation is valid for flows with boundary layer thickness much smaller than the Stokes' length, $\delta \ll \delta_s$ and is somewhat more complicated and will not be presented in this report. Concerning the thermal response, the solution given by Lighthill is limited to the flow past a circular cylinder in regions without detachment.

The linear analysis of Lighthill is restricted to small velocity amplitudes and constant thermal boundary conditions, in which no enhanced heat transfer could be predicted. Thus, for the explanation of enhanced heat transfer under less restrictive conditions, additional approaches are needed. Nevertheless, the basic behaviour of pulsating flows is properly described.

Harmonic decomposition

As already exemplified by the studies of Stokes and Lighthill, the decomposition into harmonic orders is suitable for the investigation of pulsating flows. The general decomposition up to order N can be achieved by a truncated Fourier series decomposition of the transient quantities:

$$\langle a(t)\rangle_N = a_0 + a_1 \sin(\omega t + \phi_1) + a_2 \sin(2\omega t + \phi_2) + \ldots$$
$$= \sum_{n=0}^{N} a_n \sin(n\omega t + \phi_n) \quad . \tag{12}$$

Following this notation, several effects present in pulsating flows can be defined. The secondary flows u_{str} induced by viscous forces, the so called “streaming”, can be written after the decomposition as:

$$u_{str} = u_0 - u_{stat} \quad , \tag{13}$$

where u_{stat} represents the velocity of the unperturbed stationary case. Concerning the energy transfer, the heat transfer enhancement can be defined as

$$EHT = \frac{\dot{q}_{w,0}}{\dot{q}_{stat}} \quad . \tag{14}$$

SIMULATION DOMAIN AND SOLVER PROPERTIES

The two dimensional case of pulsating flow past a flat plate has been chosen for the numerical investigations. Figure 2 depicts a sketch of the simulation domain. A flat plate of length L with no slip condition and surface temperature T_w is placed far enough from the boundaries in order to avoid distortion effects at times of flow reversal. The coordinate system is placed at the beginning of the plate. At the inlet the bulk velocity with time average value of U_0, harmonic oscillations of order ϵ_u,

frequency ω and the constant bulk temperature T_{in} are imposed, while the outlet is kept at constant pressure with zero gradient for the temperature. For reasons of accuracy and since the flow is treated as incompressible, a relative pressure of $p = 0$ is chosen. For high amplitude ratios, when flow reversal occurs, the temperature boundary condition of these two patches switches.

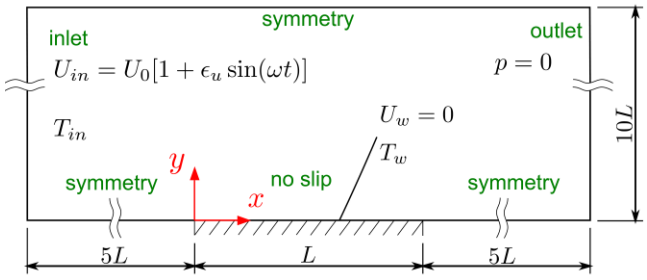

Figure 2 Sketch of simulation domain for pulsating flow past a flat plate.

For generality, consider now the system of equations (1) and (2) in dimensionless form using the substitutions $t^* = t\omega$, $\xi = x\omega/U_0$, $\zeta = y\omega/U_0$, $\vec{u}^* = \vec{u}/U_0$, $p^* = p/(\nu\rho\omega)$ and $T^* = (T_w - T)/(T_w - T_{in})$:

$$\frac{\partial \vec{u}^*}{\partial t^*} + (\vec{u}^* \cdot \vec{\nabla}^*)\vec{u}^* = \frac{\mathrm{Sr}_s}{\mathrm{Re}_s}\left[-\vec{\nabla}^* p^* + \vec{\nabla}^{*2}\vec{u}^*\right] \quad , \qquad (15)$$

$$\frac{\partial T^*}{\partial t^*} + (\vec{u}^* \cdot \vec{\nabla}^*)T^* = \frac{\mathrm{Sr}_s}{\mathrm{PrRe}_s}\vec{\nabla}^{*2}T^* \quad , \qquad (16)$$

where the Strouhal $\mathrm{Sr}_s = \delta_s\omega/U_0$ and Reynolds numbers $\mathrm{Re}_s = \delta_s U_0/\nu$ based on the Stokes' length have been introduced. The chosen dimensionless coordinate represents a local Strouhal number $\xi \sim \delta/\delta_s$, which gives the ratio of boundary layer thickness to Stokes' length. The boundary layer grows unobstructedly along the plate, and thus, for a given frequency ω, the low frequency regime is expected near to the left stagnation point, while far from it the high frequency regime appears.

The skin friction and wall heat flux have been nondimensionalized by:

$$\tau_w^* = \frac{\tau_w}{\mu\omega} \quad , \quad \dot{q}_w^* = \frac{\dot{q}_w}{c_p\rho(T_w - T_{in})} \quad . \qquad (17)$$

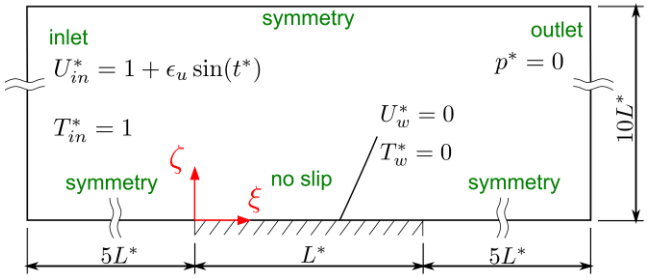

Figure 3 Sketch of simulation domain in dimensionless form.

For clarity, **Figure 3** depicts the sketch of the simulation domain with the applied boundary conditions in their dimensionless form. The imposed bulk velocity at the inlet has now the form $U_{in}^* = 1 + \epsilon_u \sin(t^*)$. Note that the wall temperature has a value $T_w^* = 0$, while the bulk temperature a value of $T_{in}^* = 1$. The coordinate system placed at the beginning of the plate represents in the streamwise direction the local Strouhal number ξ.

For the numerical solution of the problem, the open-source package openFOAM ("Open Field Operation and Manipulation") has been chosen. Written in C++ and build upon common object-orientation techniques, the package provides a general code, that uses a top-level syntax very close to conventional partial differential equations in order to facilitate the programming and extension of solvers [10]. In openFOAM, the system of partial differential equations has been discretized into finite volumes and solved iteratively with the PISO ("Pressure Implicit with Splitting of Operators") method, which is an implicit pressure based algorithm performing two momentum corrector steps [11].

The simulation domain has been spatially discretized by a non-uniform unstructured hexahedral mesh with a total number of 70091 cells. For the heated plate of length L a number of 249 cells have been used. In the wall normal direction, 133 cells with an expansion ratio of 1.0607 have been used. For the time integration, the second order Crank-Nicholson scheme has been used. Spatial discretization of the convective fluxes is performed through a second order Gauss scheme, for which the face fluxes are interpolated through a second order upwind differencing scheme limited by a Van Leer function. The diffusive fluxes are discretized through a second order Gauss scheme, for which the surface normal gradients are interpolated through a second order upwind differencing scheme. For pressure and velocity, the iterations are stopped for residuals lower than 10^{-6}, while for the temperature 10^{-11} is used.

Solver and domain setup have been first validated by a stationary test case without any pulsations. This case served as well as a reference to compare and define the ratio of heat transfer enhancement. The resolution of the mesh proved to be fine enough to resolve the boundary layer, both thermally and hydrodynamically. This has been proved comparing the velocity profiles of the stationary test case against well-known analytical solutions, e.g. Karman and Pohlhausen [8]. The integration errors of the solver for mass and energy conservation lie below 0.3%. The temperature range used in all simulations is small enough so the passive scalar simplification for the temperature remains valid.

	Reference	Const. T_w	Osc. T_w
Pr	0.7	0.7	0.7
Re_s	27	27	27
Sr_s	0.036	0.036	0.036
L^*	0.38	0.38	0.38
ϵ_u	0	0.1 - 2.5	1.25
ϵ_T	0	0	0.1 - 1.25

Table 1 Simulation parameters for the reference case and the two simulation campaigns.

Table 1 gives a brief overview of the parameter ranges studied in this paper: the reference case, a simulation campaign with constant thermal boundary conditions and a second campaign with oscillating surface wall temperature that emulates the effects of oscillating thermal boundary conditions. This second thermal boundary condition will be explained later on.

PULSATING FLOW, CONSTANT TEMPERATURE

The case with constant wall temperature $T_w^* = 0$ will be studied first. Before treating the heat transfer in flows with high velocity fluctuations, the simulation setup has been validated against the analytical solution of Lighthill for small amplitudes where second order terms in the fluctuating quantities are negligible small.

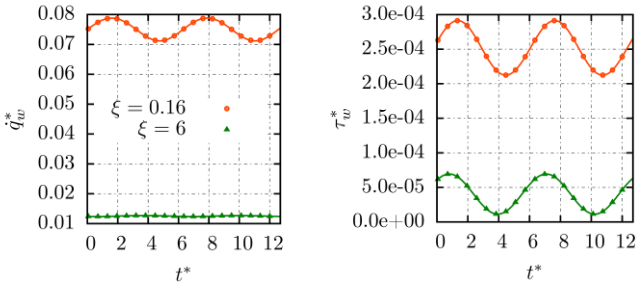

Figure 4 Temporal dependency of skin friction and heat flux for two points corresponding to low (ξ=0.16) and high (ξ=6) frequency regime. Small amplitude ratio $\epsilon_u = 0.1$.

Low amplitude ratios

To validate the solver and test case set up in the pulsating case, a first transient simulation with small amplitude ratio $\epsilon_u = 0.1$ has been performed and compared against the analytical solution of Lighthill. Two monitoring points placed one in the low- ($\xi = 0.16$) and a second in the high-frequency region ($\xi = 6$) are used to verify the linear behaviour of the skin friction and the heat flux respectively. Figure 4 shows the temporal dependency of u^* and T^* at these monitoring points. The first order approximation suggested by Lighthill is clearly sufficient to describe the dynamic behaviour.

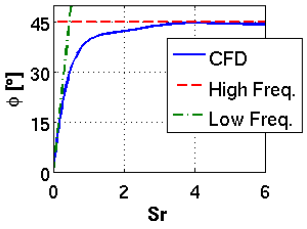

Figure 5 Skin friction phase along the plate for constant frequency and amplitude ratio $\boldsymbol{\epsilon_u = 0.1}$. Dashed lines denote Lighthill's approximation.

Figure 5 shows the skin friction phase shift ϕ plotted against the frequency parameter ξ along the surface of the plate. As expected, it starts with a value of 0 and increases until it reaches the maximum value of $\pi/4$ confirming the possibility of having both frequency regimes in one simulation [7]. The dashed lines correspond to Lighthill's high and low frequency approximations respectively. The high frequency regime is clearly displayed at frequency parameter > 4 . Figure 6 shows the phase ϕ and gain $g = u(\eta)/U_0$ of the boundary layer velocity at this location plotted against local wall units $= y\sqrt{\frac{U_0}{\nu x}} \sim \frac{y}{\delta}$. In the high frequency regime, the velocity fluctuations in the boundary layer have phase advance starting with $\pi/2$ just above the wall. The phase shift decreases with distance to the wall and reaches the value 0 as expected at the end of the local boundary layer $\eta = 1$. Due to its lower inertia, the fluid near the wall reacts faster to the fluctuations than the external flow. As can be seen in Figure 6 the velocity fluctuation gain grows with distance to the wall and reaches its maximum shortly before the end of the boundary layer. It has a small overshoot before it reaches the expected value of 1 far away from the wall.

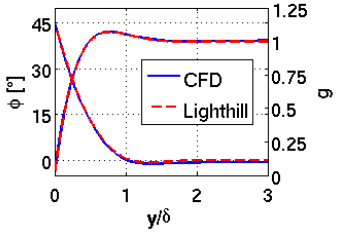

Figure 6 Gain and phase of skin friction in the high frequency regime with an amplitude ratio $\boldsymbol{\epsilon_u = 0.1}$. Dashed lines represent Lighthill's high frequency approximation.

High amplitude ratios

After validating the solver and test case, several simulations at different amplitude ratios have been then conducted, see Table 1. Especially at amplitude ratios $\epsilon_u > 1$ when flow reversal occurs, the linear behaviour of the skin friction and the heat flux is no longer valid throughout the whole plate. Figure 7 shows the corresponding temporal dependency of skin friction and wall heat flux at the monitoring points for a velocity amplitude ration of $\epsilon_u = 2.5$, where higher harmonics can be clearly observed. These nonlinearities are considerably stronger at the leading edge of the plate. In the low frequency regime the Stokes layer resides in a region with strong axial gradients of temperature and velocity. The pulsations have then a stronger impact on the local transfer of heat and momentum. Far from the leading edge, in the high frequency regime, the Stokes layer resides deep inside the boundary layer, where the axial dependency is marginarly. The perturbations are small and thus, the impact on the energy and momentum transfer remains linear.

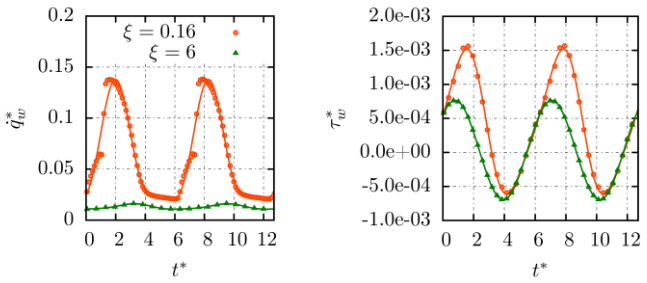

Figure 7 Temporal dependency of skin friction and heat flux at the monitoring points for an amplitude ratio of $\epsilon_u = 2.5$.

A decomposition up to second harmonic order provides a satisfactory approximation of the temporal profiles.

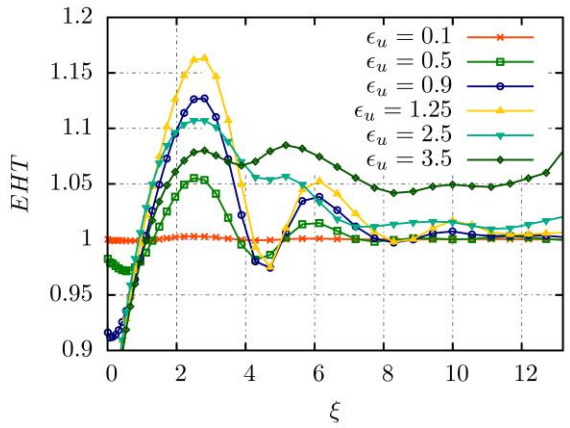

Figure 8 Enhanced heat transfer for different amplitude ratios and constant plate temperature.

Since we are interested in the heat transfer in pulsating flows, the main results of the investigation can be expressed in terms of the previously defined *EHT* ratio. Figure 8 gives the local ratio of enhancement along the plate in terms of the frequency parameter ξ for different amplitude ratios ϵ_u. It is interesting to note that regions of locally enhanced as well as decreased heat transfer are present, with a periodic dependency in axial direction in accordance to the results of Hemida et al. [4]. As expected, the heat flux perturbations are stronger near the leading edge in the thermally developing region. Further downstream the perturbations are damped out.

Up to an amplitude ratio of approximately $\epsilon_u \approx 1.75$ the enhancement is proportional to the amplitude ratio ϵ_u and its periodic behaviour similar, with maxima and minima located at the same ξ's. This behaviour can be approximately described by the following function:

$$EHT \sim 1 + \epsilon_u e^{-\alpha\xi} \sin(\beta\xi + \gamma) \quad . \qquad (18)$$

For higher amplitude ratios $\epsilon_u > 1.75$ a nonlinear mechanism present at higher amplitude ratios start to play a role; the axial periodicity is broken and the magnitude of the perturbations decay again. The reason for this behaviour will be explained later on. Finally, for the frequency range considered, the maximum enhancement found was about $EHT \approx 1.17$ for an amplitude ratio of $\epsilon_u \approx 1.25$ at position $\xi \approx 2.6$.

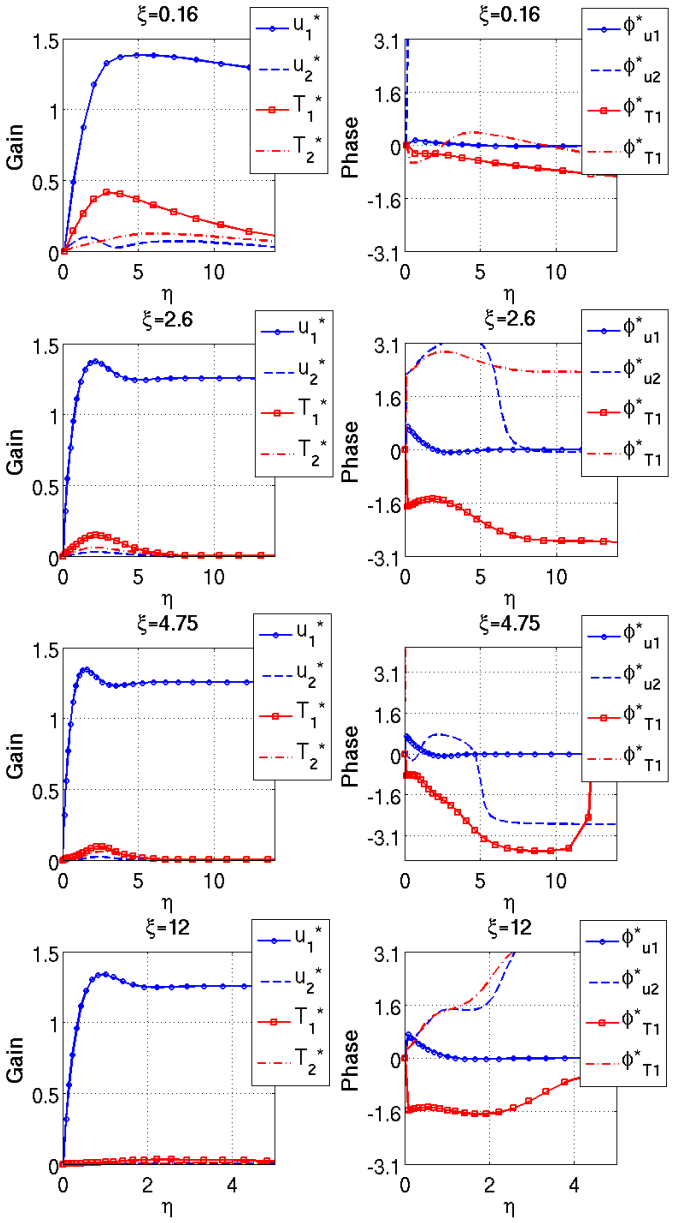

Figure 9 Gain and phase at different plate positions $\boldsymbol{\xi}$ for pulsations of order $\epsilon_u = 1.25$ and constant wall temperature.

Four characteristic axial locations have been chosen for the interpretation of the results. The first one at location $\xi = 0.16$, which, according to Figure 5, resides in the low frequency regime. The second position lies at $\xi = 2.6$, where the strongest enhancement is observed. Position $\xi = 4.75$ is close to a local minimum. At position $\xi = 12$ the perturbations of the *EHT* are almost completely damped out. **Error! Reference source not found.** show the corresponding gain and phase diagrams.

The simplest case is that at position $\xi = 12$. The thermal boundary layer is so far developed, at least in the region

covered by the Stokes' length. The axial gradients are marginal inside it and no temperature fluctuations are induced. If only velocity fluctuations are present, the periods of high energy transport at faster velocities are compensated by the following periods of low energy transport with slower velocities. Under these conditions it is clear that no time average enhancement can occur.

The other three cases are more complicated. Since the periodic behaviour is present at low amplitude ratios ϵ_u too, the fundamental harmonics u_1^* and T_1^* are supposed to be responsible for the effect. While u_1^* remains more or less constant, the temperature fluctuations T_1^* decay in amplitude along the plate. The decay parameter α in the *EHT* correlates thus with the magnitude of T_1^*.

The wave length of the periodic oscillations is described approximately by the parameter β in equation (18). The driving force for the heat transfer is the temperature normal gradient at the wall. Due to the choice of normalization, the heat transfer flux points in the same direction as the gradient:

$$\dot{q}_w \sim \left.\frac{\partial T^*}{\partial \zeta}\right|_{\zeta=0} \approx \left.\frac{\partial T_1^*}{\partial \zeta}\right|_{\zeta=0} \sin(t^* + \phi_{T1}) \qquad (19)$$

and correlates with the fundamental harmonic of the temperature fluctuations. A steep temperature normal gradient means that the fluid near the wall is not yet heated up and a flat gradient means that the fluid is saturated.

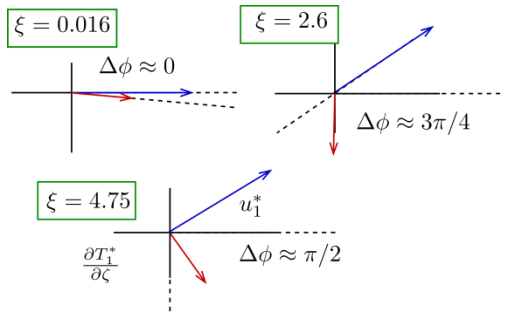

Figure 10 Polar diagram of temperature normal gradient and velocity fluctuations (fundamental harmonic).

We give a similar explanation as Hemida et al. [4]: if the temperature fluctuates in such a way that a steep gradient is present at times of low velocity, the fluid just above the wall will start to heat up. Before starting to saturate, the velocity would then start to increase again and the heat transfer will not be inhibited at times of low velocity. The phase difference between T_1^* and u_1^* at the plate surface takes the decisive role.

Error! Reference source not found. shows schematically the phase lags in the three previously mentioned locations in a polar diagram. At the first position $\xi = 0.016$, the temperature gradient and the velocity are in face, see Figure 9. Thus, at times of low velocities, the temperature gradient will be flat, which means that the fluid is already heated up and none energy transport will occur, leading to the heat transfer decrease at this position. The second position at $\xi = 2.6$, displays a phase difference of nearly $3\pi/4$. Even if not at its ideal maximum, the temperature gradient will still be steeper than in the reference case at times of low velocity. Thus, the heat transfer enhancement occurs. The third position at $\xi = 4.75$ shows a case where the phase shift between the pulsations is nearly $/2$. In such a case, the temperature gradient will be the same as in the stationary case at times of higher or lower velocities. Thus the two periods will compensate, and the discrepancy towards the stationary case will be marginal, as can be seen in Figure 8.

At higher amplitude ratios $\epsilon_u > 1.75$, the dependency of *EHT* on ξ start to change with the maxima and minima being softened leading to a decrease in magnitude of the enhancement. At high amplitude ratios with strong flow reversal, secondary flows ("streaming") appear. Their structure depends on the overall geometry and the location of the stagnation points [12]. In the geometry used for this study, this secondary flows reduce the velocity at the boundary layer near to the leading edge of the plate, see Figure 11, where the time independent coefficients u_0 of the Fourier decomposition are plotted for different amplitude ratios. This reduction in the wall normal velocity gradient counteracts with the mechanism responsible for the enhancement.

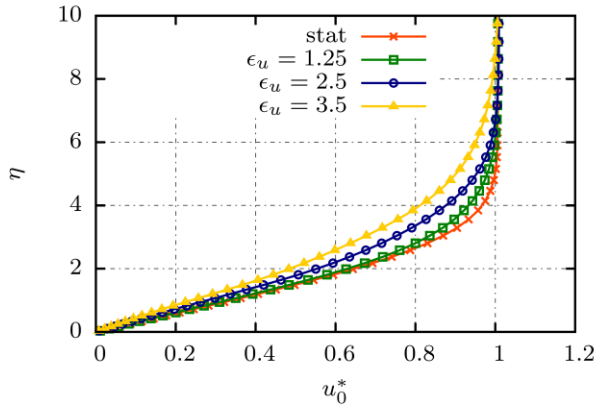

Figure 11 Time independent terms of the ensemble averaging for the velocity.

PULSATING FLOW, VARIABLE WALL TEMPERATURE

In devices where enhanced heat transfer has been observed, it can be expected that temperature fluctuations occur in addition to the ones of velocity, too. For example, the bulk temperature of the fluid might oscillate due to combustion instabilities. In order to estimate the effects of these temperature fluctuations on the heat transfer, transient thermal boundary conditions have to be used. Inducing the temperature fluctuations at the inlet or outlet patches would not be appropriate, since they are placed far away from the plate. Due to diffusion, the perturbations would be damped out before reaching the heated plate. Instead, a generalized thermal wall boundary condition is introduced:

$$T_w^* = \epsilon_T \sin(t^* + \psi) \quad . \qquad (20)$$

The wall temperature oscillates around a zero mean value with the same frequency as the velocity fluctuations, but with a possible phase shift ψ. In most devices prone to thermoacoustic oscillations, like the tail pipe of a pulse combustor [1], the

phase shift between temperature and velocity fluctuations is about $\psi = \pi/2$. This value is used for the investigation.

To account for the impact of such a fluctuation, a second simulation campaign has been conducted, see Table 1. The case with a velocity amplitude ration of $\epsilon_u = 1.25$ has been repeated for several temperature amplitudes. Figure 12 shows the result concerning the ratio of enhancement. The same periodic character as in the previous simulation campaign is given. However, the amplitude values of EHT are gradually increased. The temperature fluctuations of the plate occur thus at the proper phase in order to support the previously mentioned interaction near the plate surface. It is interesting to note, that fluctuations of the wall temperature with different phase shift ψ might lead to exactly the opposite effect. This behaviour has been studied analytically by Emmert et al. [13] with a low order model.

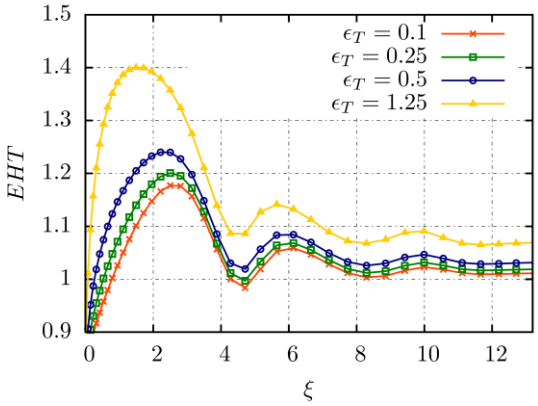

Figure 12 EHT for different temperature amplitude ratios ϵ_T and constant velocity amplitude ratio of $\epsilon_u = 1.25$.

CONCLUSIONS

In this study, the laminar pulsating flow past a heated flat plate has been studied numerically. A locally defined Strouhal number and local ratio of hydrodynamic versus Stokes' layer characterizes the frequency regime along the plate. For a given forcing frequency, it changes gradually from the low into the high frequency regime. A wide range of velocity amplitude ratios and Strouhal number covering flow reversal have been used in the investigation. Compared to the stationary reference case, the heat transfer alternatively increases and decreases. The amplitude of these perturbations decays along the plate. These two observations are in accordance with previous results reported in the literature. In the thermally developed region the amplitudes of the temperature fluctuations are stronger and thus, the impact on the heat transfer is higher. The phase shift between velocity and temperature fluctuations close to the wall surface is responsible for the periodic character. At high velocity amplitude ratios, the characteristic of the enhancement changes. Secondary stationary flows called "streaming" appear near the stagnation points and are responsible for this behaviour. In addition, and in contrast to previous investigations transient periodic thermal boundary conditions were also studied for different Strouhal numbers. An oscillating wall temperature was chosen to take these effects into account. The phase shift between bulk velocity and wall temperature oscillations decides whether the enhancement is supported or not. A phase shift of $\pi/2$ appears to be favourable for enhanced heat transfer.

ACKNOWLEDGMENTS

Financial support has been provided by the German Research Foundation (Deutsche Forschungsgemeinschaft -- DFG) in the framework of the Sonderforschungsbereich Transregio 40.

REFERENCES

[1] DEC, J.E., KELLER, J.O. AND ARPACI, V.S. (1992). Heat transfer enhancement in the oscillating turbulent flow of a pulse combustor tail pipe. *International Journal of Heat and Mass Transfer*, **35**,(9) 2311–2325.

[2] PERRY, E.H. AND CULICK, F.E.C. (1974). Measurements of wall heat transfer in the presence of large-amplitude combustion-driven oscillations. *Combustion Science and Technology*, **9**,(1) 49–53.

[3] HOLST, A., LUNDGREN, E. AND MARKSTEN, U. (2002). Measurements of wall heat transfer in the presence of large-amplitude combustion-driven oscillations. *American Society of Mechanical Engineers, Heat Transfer Division,(Publication) HTD*, **372**,(2) 89–53.

[4] HEMIDA, H.N., SABRY, M.N., ABDEL-RAHIM, A. AND MANSOUR, H.E., (2002). Theoretical analysis of heat transfer in laminar pulsating flow. *International Journal of Heat and Mass Transfer*, **45**,(9) 1767-1780.

[5] HABIB, M.A., ATTYA, A.M., EID, A.I. AND ALY, A.Z. (2002). Convective heat transfer characteristics of laminar pulsating pipe air flow. *Heat and Mass Transfer*, **38**, 221–232.

[6] GUNDOGDU, M.Y. AND CARPINLIOGLU, M.O. (1999). Present State of Art on Pulsatile Flow Theory: Part 1: Laminar and Transitional Flow Regimes. *JSME international journal. Ser. B, Fluids and thermal engineering*, **42**,(3) 384–397.

[7] TELIONIS, D.P. (1981). *Unsteady viscous flows.* Springer Series in Computational Physics.

[8] GOLDSTEIN, S. (1950). *Modern developments in fluid mechanics, Vol. I.* Oxford at the Claredon Press.

[9] LIGHTHILL, M.J. (1954). The response of laminar skin friction and heat transfer to fluctuations in the stream velocity. *Proceedings of the Royal Society of London. Series A. Mathematical and Physical Sciences*, **224**,(1156) 1–23.

[10] WELLER, H.G., TABOR, G., JASAK, H. AND FUREBY, C. (1998). A tensorial approach to computational continuum mechanics using object-oriented techniques. *Computers in Physics*, **12**,(6) 620–631.

[11] ISSA, R.I. (1986). Solution of the implicitly discretised fluid flow equations by operator-splitting. *Journal of Computational physics*, **62**,(1) 40–65.

[12] RILEY, N. (2001) Steady streaming. *Annual Review of Fluid Mechanics*, **33**, 43-65.

[13] EMMERT, T., CARDENAS, A. AND POLIFKE, W. (2012). Low-Order analysis of conjugate heat transfer in pulsating flow with fluctuating temperature. *In preparation for publication in the 6th European Thermal Sciences Conference, EUROTHERM.* Poitiers - Futuroscope France.